Modelling Wave Interaction with Deformable Structures based on a Multi-region Approach within OpenFOAM

P. J. Martínez Ferrer, L. Qian, Z. Ma, D. Causon, C. Mingham
Centre for Mathematical Modelling and Flow Analysis
Manchester Metropolitan University
Chester Street, Manchester M1 5GD, United Kingdom

ABSTRACT

This paper presents the development of a multi-region computational fluid-structure dynamics (CFSD) method which is integrated in our virtual wave structure interaction solver wsiFoam, based on the open-source OpenFOAM library, in order to account for the hydro-elastic effects produced by violent wave impacts against deformable bodies. This strategy relies entirely on the finite volume method (FVM) and does not require any third-party solvers, which renders it suitable for efficient parallel computing. We validate this novel approach against previous experimental and numerical results corresponding to a dam break of water impacting on a highly deformable plate as well as a flexible wedge entering water at a constant speed. In general, our preliminary results agree qualitatively well with previous data whilst the performance of parallel implementation evidences the potential of this method to be used in future high performing computing (HPC) applications.

KEY WORDS: fluid structure interaction, hydroelasticity, wave impact

INTRODUCTION

Wave impacts are characteristic of marine engineering problems. Floating platforms, ships and LNG tanks can experience frequent wave impacts in high sea states. The local and stochastic nature of wave impact loads due to free surface instabilities makes this problem difficult to study both experimentally and computationally. For example, air entrapment may occur when the impact angle between the water and the structure is small. Considering only fluid dynamics aspects, the air compressibility may play an important role in such conditions leading to a further increase in the maximum impact pressure (Bullock et al. 2007, Lugni et al. 2010, Ma et al. 2016), which can compromise the integrity of the structure.

On the other hand, wave impact is often a fluid-structure interaction problem between the free surface flow and an elastic structure. A recent experiment carried out using rigid (steel) and elastic (aluminium) plates showed the important role of hydro-elasticity during the evolution of a flip-through event in a low filled sloshing tank (Lugni et al. 2014). When the elastic plate deforms against the incoming wave, the impact pressure increases almost by a factor of 2 with respect the case where a rigid plate is used; subsequent pressure oscillations are also produced, thus revealing a strong hydro-elastic effect.

The vast majority of the computational works related to wave impacts still concentrate on the fluid dynamics behaviour on rigid structures thus neglecting the important hydro-elastic effects. Different approaches to deal with fluid-structure interaction (FSI) and to account for hydro-elasticity can be found in the literature (Hou et al. 2012). Traditionally, FSI involves a combination of three tools: a finite volume solver for the fluid, a finite element solver for the structure and, finally, a third code to couple the previous two solvers and manage the data exchange between them. This methodology suffers from a lot of limitations such as model setup and coupling. Furthermore, with the continuous growth of large scale simulations and HPC applications, these strategies become rapidly obsolete, especially if the data exchange is not carried out using fast random-access memory.

Although the finite element method is widely used for structural analysis (Bathe & Hahn 1979), the FVM has been gaining popularity to solve computer structure dynamics (CSD) problems due to its memory efficiency (Jasak & Weller 2000). The present work relies on the FVM provided by OpenFOAM to solve both the fluid and solid in an unified, partitioned framework in order to account for hydroelasticity phenomena whilst allowing the possibility to use HPC resources for large scale applications.

The present paper is organised as follows. We firstly describe the numerical methods and the implementation of the FSI strategy for the simulation of violent wave impacts characteristic of ocean and coastal engineering applications. Then we test two experimental configurations corresponding to (i) a dam break of water impacting on an elastic plate and (ii) a flexible wedge entering water at a constant speed. Conclusions and further work are provided at the end of this document.

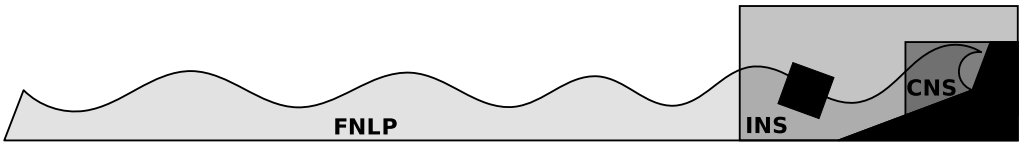

Fig. 1 Multi-region virtual wave structure interaction (WSI) simulation environment.

NUMERICAL METHOD

Our numerical procedures rely on a cell-centred, co-located finite volume method, available in the open-source CFD software OpenFOAM (Jasak 1996). We have previously developed a novel OpenFOAM-based solver, wsiFoam (Martínez Ferrer et al. 2016*a*), for the study of wave interaction between *rigid* structures and floating bodies (Martínez Ferrer et al. 2016*b*). The aim of wsiFoam is to gather specialised solvers, e.g. fully non-linear potential (FNLP), incompressible Navier-Stokes (INS) and compressible Navier-Stokes (CNS) solvers, at strategic locations of the computational domain and couple them through special interfaces in order to get the most efficient and accurate description of the underlying physics in a numerical wave tank, as schematised in Fig. 1.

We solve the fluid with the aid of an incompressible two-phase pressure-based solver (Rusche 2002), which is based on the volume of fluid (VOF) method to describe the two-phase fluid mixture, i.e. air and water, assumed to be homogeneous and in mechanical equilibrium, i.e. identical velocity and pressure. The mass balance equation of the water volume fraction $\alpha \in [0, 1]$ is given by

$$\frac{\partial \alpha}{\partial t} + \boldsymbol{\nabla} \cdot \mathbf{U}\alpha + \boldsymbol{\nabla} \cdot \mathbf{U}_\mathrm{c}\alpha(1-\alpha) = 0, \tag{1}$$

where $\mathbf{U}$ is the mixture velocity vector and $\mathbf{U}_\mathrm{c} = \min[\mathbf{U}, \max(\mathbf{U})]$. The density of the mixture is $\rho = \alpha\rho_\mathrm{w} + (1-\alpha)\rho_\mathrm{a}$; ρ_w and ρ_a are the constant partial densities of water and air, respectively. The third term in eq. (1) is an artificial compression quantity that sharpens the interface and guarantees bounded values of α by using the MULES procedure (Weller 2002). The single momentum equation of the homogeneous mixture is written as

$$\frac{\partial \rho \mathbf{U}}{\partial t} + \boldsymbol{\nabla} \cdot (\rho \mathbf{U}\mathbf{U}) - \boldsymbol{\nabla} \cdot (\mu \boldsymbol{\nabla} \mathbf{U}) = \sigma\kappa\boldsymbol{\nabla}\alpha - \mathbf{g} \cdot \mathbf{x}\boldsymbol{\nabla}\rho - \boldsymbol{\nabla} p_\mathrm{d}, \tag{2}$$

where σ denotes the surface tension coefficient and $\kappa = \boldsymbol{\nabla} \cdot (\boldsymbol{\nabla}\alpha/|\boldsymbol{\nabla}\alpha|)$ represents the curvature of the interface. The mixture viscosity is given by $\mu = \alpha\mu_\mathrm{w} + (1-\alpha)\mu_\mathrm{a}$ and the dynamic pressure is calculated as $p_\mathrm{d} = p - \rho\mathbf{g} \cdot \mathbf{x}$ with $\mathbf{g}$ and $\mathbf{x}$ the gravity and position vectors, respectively. Finally, the governing equations (1)–(2) are linearised and integrated over each control volume to determine α and $\mathbf{U}$, respectively, and a pressure corrector linearised equation is solved for p_d. This solution procedure relies on the segregated projection algorithm PIMPLE (Kissling et al. 2010).

The solid equations are solved using the FVM strategy described by Jasak & Weller (2000), Tukovic & Jasak (2007), Tukovic et al. (2013). This approach constitutes a fast and memory-efficient alternative to well-established finite element solvers and can be easily parallelised for HPC applications. The structure is assumed to be elastic and compressible and the equation for the displacement vector $\mathbf{u}$ written with respect to the initial, i.e. undeformed, configuration is

$$\rho_\mathrm{s} \frac{\partial^2 \mathbf{u}}{\partial t^2} = \boldsymbol{\nabla} \cdot \left(\boldsymbol{\Sigma}\mathbf{F}^\mathrm{T}\right), \tag{3}$$

where ρ_s is the solid density, $\mathbf{F} = \mathbf{I} + (\boldsymbol{\nabla}\mathbf{u})^\mathrm{T}$ the deformation gradient tensor, $\boldsymbol{\Sigma} = 2\mu_\mathrm{s}\mathbf{E} + \lambda_\mathrm{s}\,\mathrm{tr}(\mathbf{E})\mathbf{I}$ the second Piola-Kirchhoff stress tensor and $\mathbf{E} = (\mathbf{F}^\mathrm{T} \cdot \mathbf{F} - \mathbf{I})/2$ represents the Green-Lagrangian strain tensor. The Lamé coefficients are defined as $\mu_\mathrm{s} = E/[2(1+\nu_\mathrm{s})]$ and $\lambda_\mathrm{s} = \nu_\mathrm{s}E/[(1+\nu_\mathrm{s})(1-2\nu_\mathrm{s})]$, respectively, where E denotes the Young's modulus and ν_s the Poisson ratio. For further details see Tukovic & Jasak (2007).

Algorithm 1: Aitken's under-relaxation method.

```
begin time advancement
    while |u_f − u_s| > ϵ do
        estimate interface displacement (Aitken);
        move fluid mesh (u_f);
        solve fluid equations;
        update solid boundary conditions;
        solve solid equation (u_s);
    end
    update the simulation time;
end
```

We utilise Aitken's under-relaxation method presented in Algorithm 1 to guarantee a strongly coupled partitioned FSI implementation. The fluid and solid meshes are treated as separated regions sharing common interfaces with appropriate boundary conditions. In this configuration, fluid and solid regions are solved alternately until dynamic equilibrium is reached. Aitken's method is used to estimate the interface displacement and move the fluid mesh accordingly. Once the fluid equations are calculated in this new mesh, the fluid force is transferred to the structural solver. The solid solver calculates the displacement of the interface and transfers it back to the fluid side. This iterative process repeats until the difference between the fluid and solid displacements meets a tolerance criteria. After this, the time is updated and this procedure repeats.

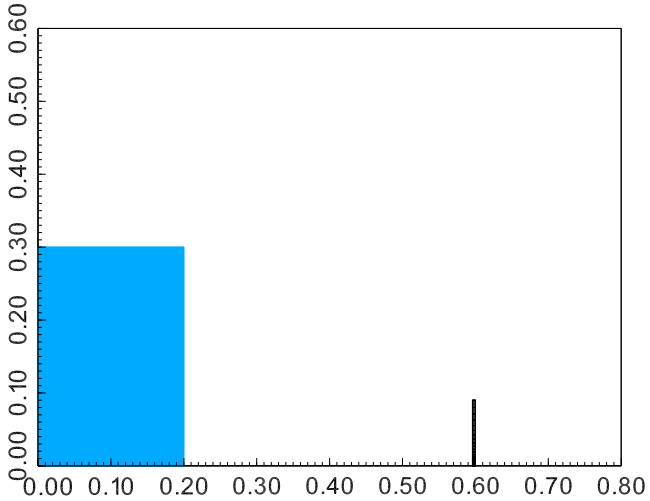

Fig. 2 Dam break impacting on an elastic plate: computational domain for $H_0 = 0.3$ m.

DAM BREAK IMPACTING ON AN ELASTIC PLATE

This experiment has been carried out at the RIAM laboratory by Liao et al. (2014, 2015) and consists of an elastic plate situated at the right hand side of a water tank and a column of water at the left hand side of variable height, i.e. $H_0 = 0.2\,\text{m}$, $H_0 = 0.3\,\text{m}$ and $H_0 = 0.4\,\text{m}$, see Fig. 2. At $t = 0\,\text{s}$ a gate holding the column of water opens and the generated flow impacts the plate, which begins to bend. The dimensions of the tank are $0.8 \times 0.6 \times 0.2\,\text{m}^3$ and the distance between the elastic plate and the right wall of the tank is 0.2 m. The plate features a thickness of 0.004 m and a height of 0.09 m. The two-dimensional fluid mesh is discretised with $82 \times 59 \times 1$ cells whilst the solid mesh is constituted of $2 \times 18 \times 1$ cells. The mesh is refined near the bottom wall and stretched above a height of 0.4 m to save computational resources. Boundaries are set as follows: the walls of the tank and the plate share a non-slip condition and the top boundary remains open to the atmosphere; the motion effect of the opening gate on the water column is not taken into account in this study. The properties of the plate, i.e. the solid, as well as water and air, i.e. the fluid, are summarised in Table 1. Finally, the simulation is run to $t = 1\,\text{s}$ with a fixed time step of $10^{-4}\,\text{s}$.

Table 1 Dam break impacting on an elastic plate: solid and fluid properties. SI units.

Property	Solid	Water	Air
Density	1161.54	997.0	1.225
K. viscosity	–	0.89×10^{-6}	0.82×10^{-5}
Young's modulus	3.5×10^6	–	–
Poisson ratio	0.48	–	–

Figs. 3–5 show snapshots taken at different times comparing the experiments of Liao et al. (2014, 2015) against our numerical results obtained with wsiFoam. Large differences can be observed in Fig. 3 corresponding to $H_0 = 0.2\,\text{m}$. At $t = 0.32\,\text{s}$ the elastic plate do not exhibit a second mode of deflection and the total displacement of the plate remains underestimated from that time onward. These differences are somewhat reduced when $H_0 = 0.3\,\text{m}$ and we obtain a good qualitative agreement for $H_0 = 0.4\,\text{m}$. The numerical results of Liao et al. (2015) also showed non-negligible qualitative discrepancies compared to the experiments. It is also worth mentioning that we were not able to capture higher orders of vibration observed during the experiments.

Figs. 6–8 show the time history of the horizontal displacement measured at the tip of the elastic plate, corresponding to the red dot in the sequence of images taken from the experiments. The differences discussed above become evident for $H_0 = 0.2\,\text{m}$, showing a maximum discrepancy of approximately 2 cm (36%) between the horizontal displacement measured in the experiment and the simulation. For $H_0 = 0.3\,\text{m}$ this difference reduces to 15% and we get closer to the numerical solution of Liao et al. (2015), which also underestimates the experiments. Indeed, both numerical solutions remain quite similar after $t = 0.35\,\text{s}$. The last case corresponding to $H_0 = 0.4\,\text{m}$ shows the best agreement between experiments and numerical simulations. The cases with $H_0 = 0.2\,\text{m}$ and $H_0 = 0.3\,\text{m}$ become more difficult to simulate due to the presence of complex and turbulent flow structures as well as the development of air cavities after the initial impact.

Finally, a negative displacement in the form of a small bump can be observed in all the experimental curves and is associated to the initial impact of the water front against the bottom of the elastic plate. As a consequence, the tip of the plate flexes towards the left as shown in Fig. 5 at $t = 0.25\,\text{s}$. Our present results tend to underestimate this early displacement. Liao et al. (2015) carried out two sets of simulations, with and without considering the influence of the gate motion, and showed an significant improvement in their numerical results when this influence was taken into account, capturing accurately negative displacements. There-

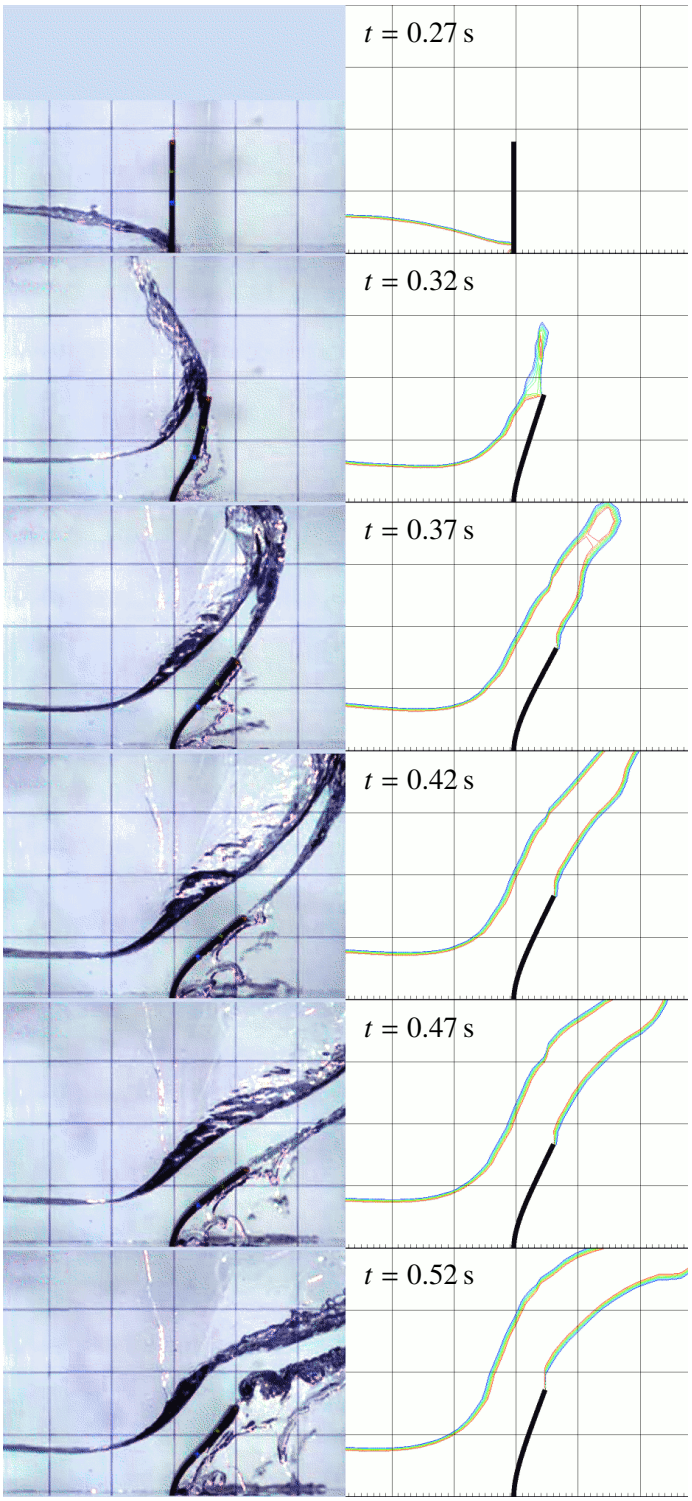

Fig. 3 Dam break impacting on an elastic plate ($H_0 = 0.2\,\text{m}$): snapshot comparison between the experiment and simulation; the blue to red rainbow palette represents ten free surface iso-contours ($0.4 \leq \alpha \leq 0.6$).

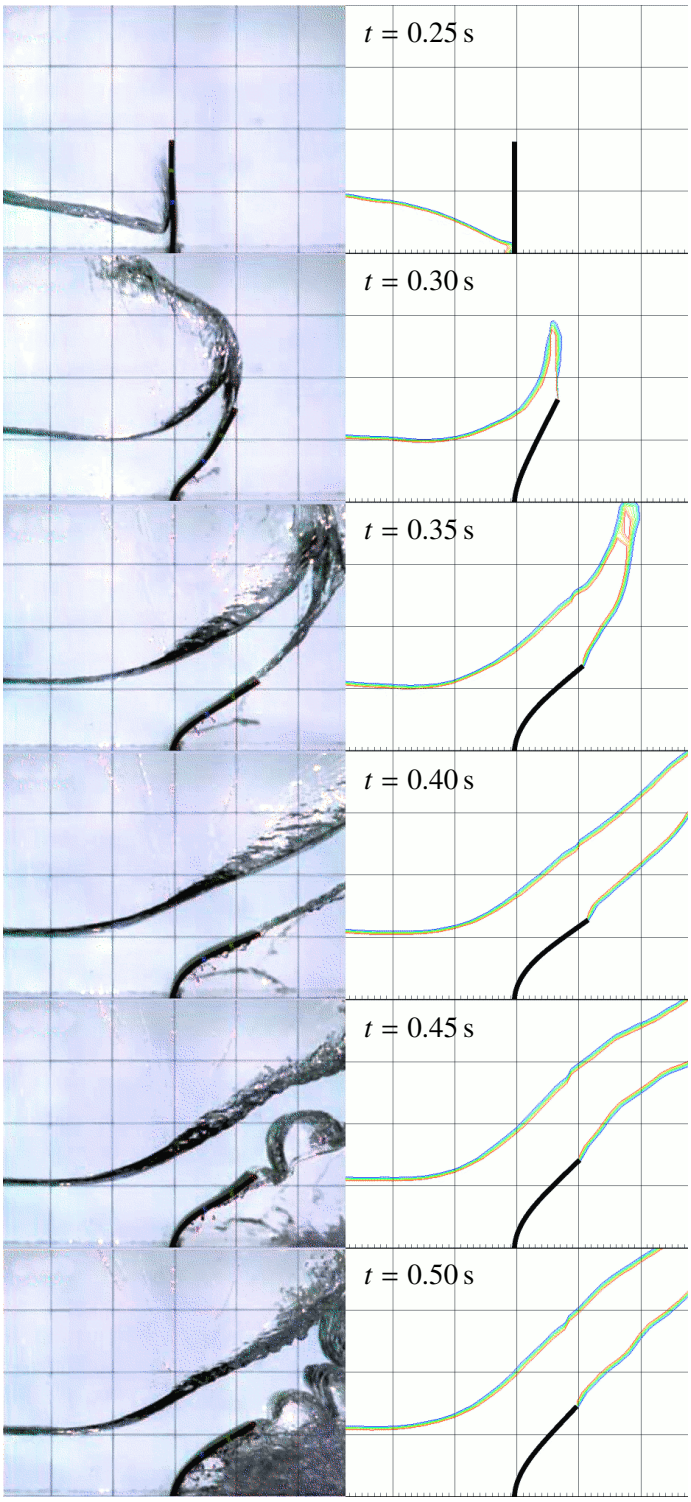

Fig. 4 Dam break impacting on an elastic plate ($H_0 = 0.3$ m): snapshot comparison between the experiment and simulation; the blue to red rainbow palette represents ten free surface iso-contours ($0.4 \leq \alpha \leq 0.6$).

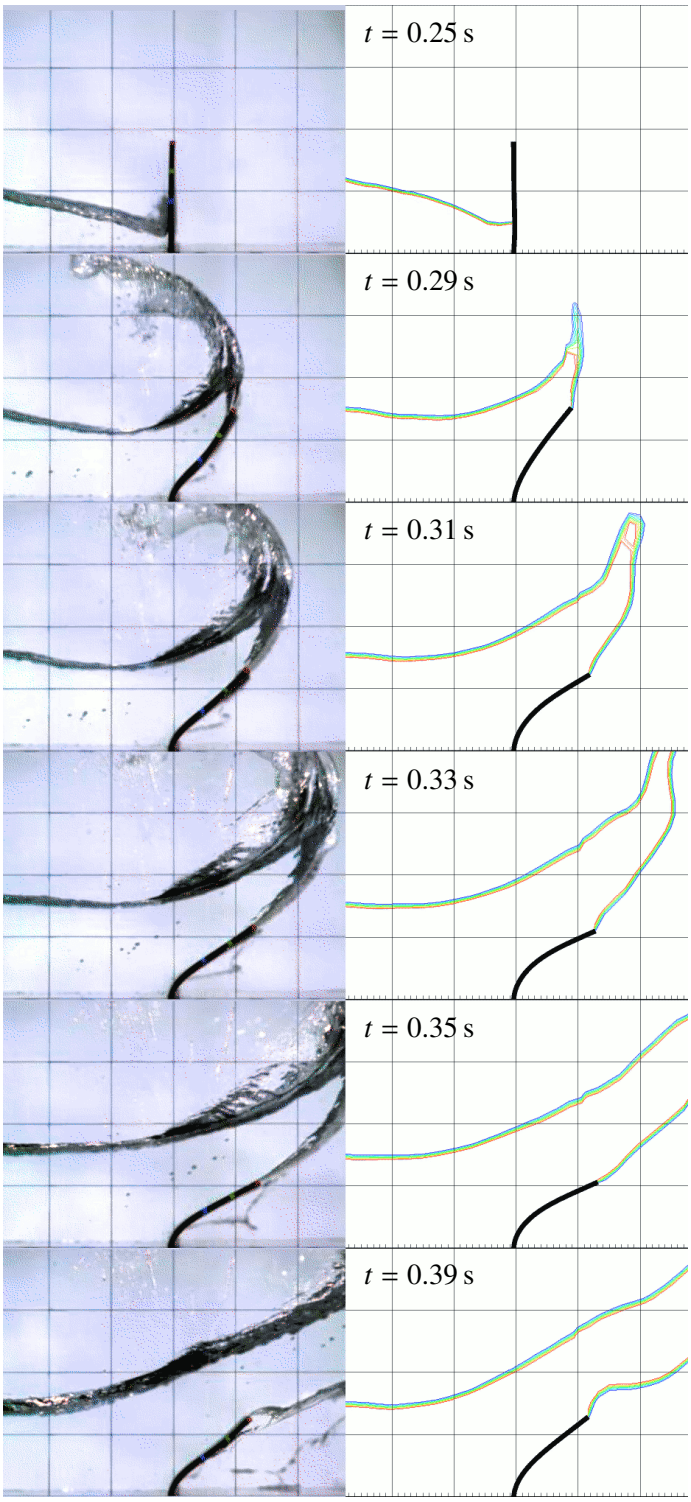

Fig. 5 Dam break impacting on an elastic plate ($H_0 = 0.4$ m): snapshot comparison between the experiment and simulation; the blue to red rainbow palette represents ten free surface iso-contours ($0.4 \leq \alpha \leq 0.6$).

fore we can expect a general improvement in our results by considering the influence of the gate.

WATER ENTRY OF RIGID AND ELASTIC WEDGES

The water entry of bodies, and in particular wedges, has been widely studied, see for instance Gu et al. (2014). An extensive analysis comparing similarity, asymptotic and numerical solutions of *rigid* wedges en-

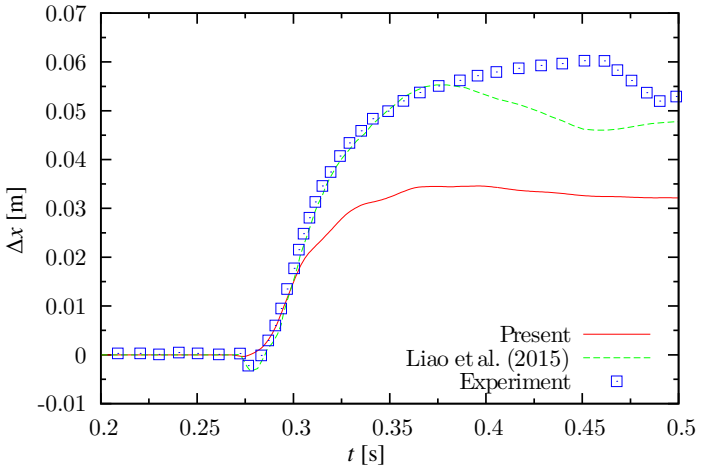

Fig. 6 Dam break impacting on an elastic plate ($H_0 = 0.2$ m): time history of the plate's tip horizontal displacement.

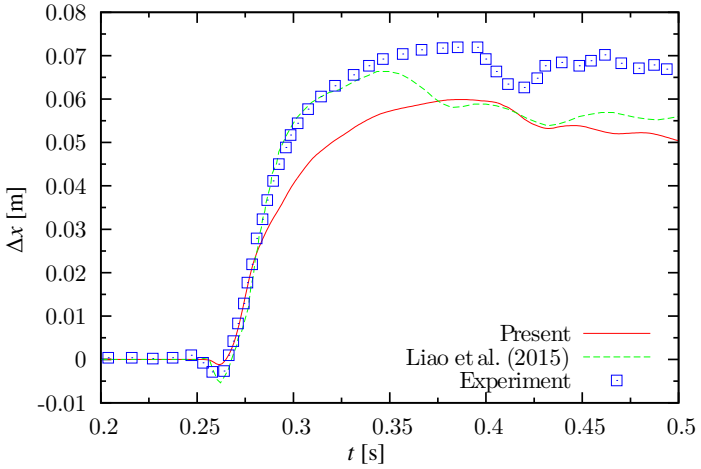

Fig. 7 Dam break impacting on an elastic plate ($H_0 = 0.3$ m): time history of the plate's tip horizontal displacement.

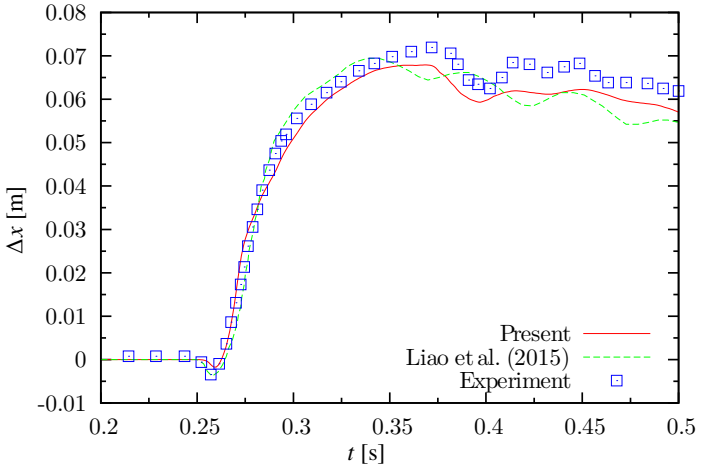

Fig. 8 Dam break impacting on an elastic plate ($H_0 = 0.4$ m): time history of the plate's tip horizontal displacement.

tering water with constant speed can be found in the early work of Zhao & Faltinsen (1993). This study was later extended by Lu et al. (2000), who considered the fluid structure interaction of the *equivalent elastic* wedge. In these two works the fluid was treated as a potential flow and

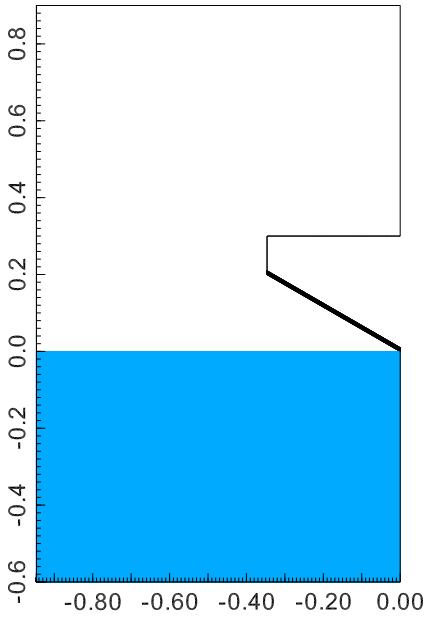

Fig. 9 Wedge water entry: computational domain.

thus the influence of the air was not taken into account. Liao et al. (2013) revisited this classic fluid structure interaction problem and considered both rigid and elastic wedges as well as the presence of air by solving the Navier-Stokes equations of a multi-phase fluid.

Table 2 Wedge water entry: solid and fluid properties. SI units.

Property	Solid	Water	Air
Density	7800	1000	1.225
K. viscosity	–	1.0×10^{-6}	0.82×10^{-5}
Young's modulus	2.0×10^{9}	–	–
Poisson ratio	0.3	–	–

The two-dimensional computational domain of dimensions $0.95 \times 1.5 \times 1\,\text{m}^3$ is shown in Fig. 9, which represents only half of the problem due to symmetry. Following Lu et al. (2000), the total height of the wedge is 0.3 m whilst the bottom measures 0.4 m and forms an angle of 30° with respect to the calm water surface. When considering a rigid wedge, FSI is deactivated and we only solve the fluid equations. Otherwise, the wedge bottom consists of a deformable plate constrained at its extremities and featuring three possible thicknesses: 5 mm, 8 mm (shown in Fig. 9) and 11 mm. All the walls of the wedge have a non-slip condition and the bottom and left domain boundaries have specified a constant value of the velocity $\mathbf{U} = (0, 1, 0)\,\text{m/s}$. Atmospheric pressure is set at the top boundary and the right domain boundaries share a symmetry condition. The properties of the solid and fluid match those specified by Liao et al. (2013), see Table 2. Finally, gravity terms are not considered in this study, which is run up to 0.2 s with a fixed time step of 10^{-5} s.

The results issued from the first set of simulations, corresponding to the *rigid* wedge, allowed us to determine the appropriate mesh discretisation in order to guarantee the convergence of our numerical solutions. Fig. 10 shows the normalised pressure distribution along the wedge bottom for three mesh configurations. Our numerical results obtained by solving the multi-phase Navier-Stokes equations are compared against previous similarity and analytical solutions based on potential theory (Lu et al. 2000). It can be readily seen that the most refined mesh, featuring 11560 cells, provides the best agreement. This body-fitted mesh is refined near the

wedge bottom ($\Delta x \approx 2.5$ mm) and stretched towards the outer boundaries where $\Delta x \approx 8$ cm. In this configuration, the solution also shows a small bump near the free-surface, which is caused by flow separation. This behaviour was previously reported by Liao et al. (2013), who associated it to gravitational terms. However, we suspect that flow detachment may be a consequence of the air motion and numerical instabilities accumulated near the interface, as we did not considered gravity in our simulations.

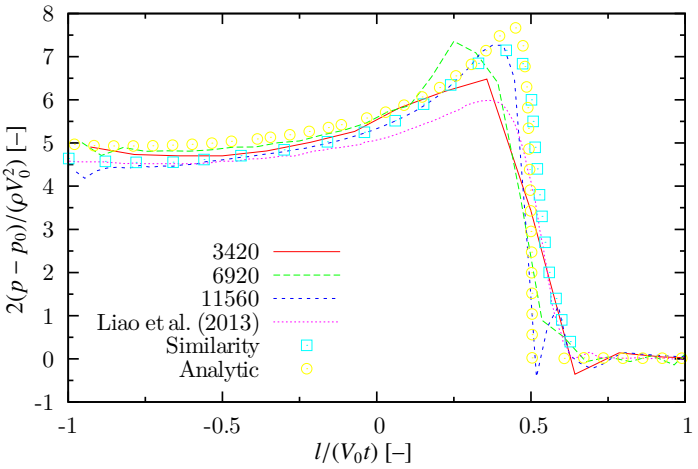

Fig. 10 Wedge water entry (rigid case): distribution of the pressure field along the wedge bottom for a different number of mesh cells.

The next set of simulations accounting for an *elastic* wedge were carried out using the same fine mesh of 11560 cells for the fluid domain whilst the solid was discretised with 160 cells. Three cases, corresponding to different plate thicknesses, were calculated. Figs. 11–13 report on the structural deflection of the wedge's bottom middle point. Our numerical results show similar trends compared to those available in the literature. Maximum deflection values are reached at nearly similar times and diminish as the plate becomes thicker. Nevertheless, the FSI partitioned strategy integrated in wsiFoam fails to retrieve values close to those reported by Lu et al. (2000) and Liao et al. (2013), specially for 8 mm and 11 mm thicknesses. Further analysis is thus required to investigate the solid mechanics solvers integrated in OpenFOAM in order to improve the solution accuracy.

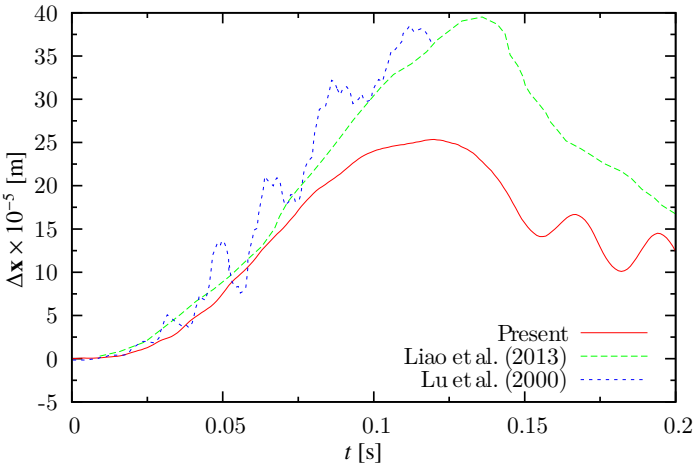

Fig. 11 Wedge water entry (elastic case): time history of the wedge's middle point displacement for 5 mm thickness.

Finally, Table 3 reports on the parallel scalability of this FSI approach. It

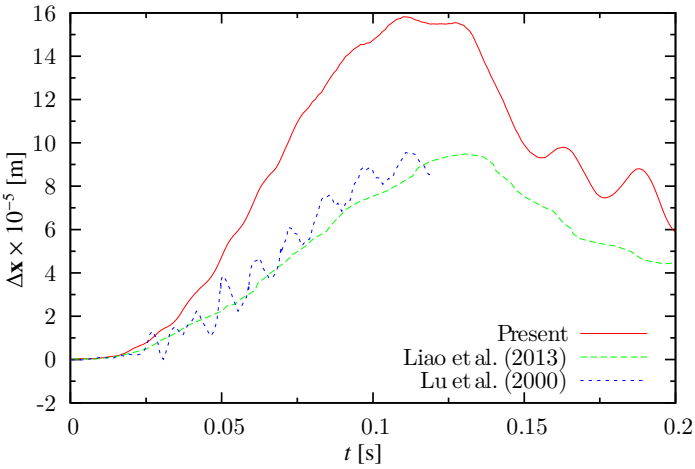

Fig. 12 Wedge water entry (elastic case): time history of the wedge's middle point displacement for 8 mm thickness.

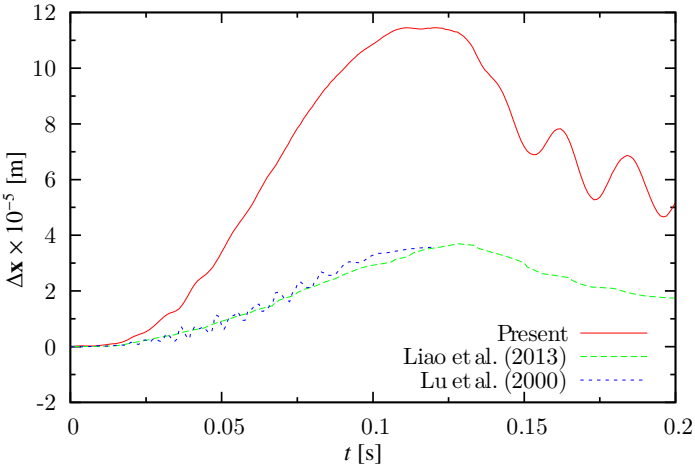

Fig. 13 Wedge water entry (elastic case): time history of the wedge's middle point displacement for 11 mm thickness.

can be readily seen that there is about an order of magnitude of difference between the solid and elastic simulation times. We get a speed up of 2.75 when using 4 cores in the rigid case. However, the elastic case exhibits a lower performance of 1.79 for the same number of cores. Such small values are expected in OpenFOAM since the number of mesh cells is relatively low: 11560 and 160 cells for the fluid and solid meshes, respectively. Therefore, greater parallel performance should be achieved for large scale computations.

Table 3 Wedge water entry: simulation speed up (t_{rm}/t)for the rigid and elastic cases; reference times corresponding to the sequential simulation are $t_{\text{ref}} = 3861$ s (rigid) and $t_{\text{ref}} = 83930$ s (elastic).

Cores	1	2	3	4
Rigid	1.00	1.72	2.33	2.75
Elastic	1.00	1.52	1.64	1.79

CONCLUSIONS

We have developed a multi-region, fluid-structure interaction procedure based on the open-source library OpenFOAM and integrated it in our

virtual wave structure interaction solver wsiFoam. It offers the flexibility of OpenFOAM as well as an unified FVM framework for the fluid and solid equations, which renders it suitable to large scale computations.

We have tested our FSI strategy in cases featuring water violent impacts. Our first numerical results, corresponding to a dam break impacting on a flexible plate, show a qualitative good agreement against experiments and previous numerical data. However, we were not able to predict higher modes of vibration with our current procedure. Large differences were also observed for the lowest height of water. These discrepancies may be caused by the influence of the gate motion used in the experiments as pointed out by other investigators.

We have also studied the water entry of rigid and flexible wedges. On the one hand, the rigid case shows good agreement against analytical and similarity solutions based on potential theory and also confirms the separation of the flow near the wedge bottom in concordance with previous works in which a multi-phase Navier-Stokes model was used. On the other hand, our results corresponding to the elastic case show similar trends to those previously reported. Nevertheless, we could not accurately predict the maximum displacements values.

Finally, we performed parallel simulations to show the capabilities of this FSI solver for HPC applications. Parallel performance was not optimal for the engineering applications considered in this work due to the relatively small number of mesh cells used. However, better performance is expected for large scale problems and thus we believe that this method is an attractive candidate for the HPC of realistic ocean and coastal engineering scenarios.

Further work will be carried out to improve the accuracy of OpenFOAM's solid mechanics solvers. A generalised grid interpolator technique between non-conformal fluid and solid meshes will be incorporated to guarantee a better FSI coupling. Finally, a compressible Navier-Stokes solver will be also considered in the future in order to account for the combined effects of compressibility and hydroelasticity during violent wave impacts.

ACKNOWLEDGEMENTS

The authors acknowledge with gratitude financial support from the Engineering and Physical Sciences Research Council (EPSRC) under the Software for the Future (SoFT) initiative and related research grants EP/K037889/1, EP/K038168/1 and EP/K038303/1.

REFERENCES

Bathe, K. & Hahn, W. (1979), 'On transient analysis of fluid-structure systems', *Computers & Structures* **10**(1-2), 383–391.

Bullock, G., Obhrai, C., Peregrine, D. & Bredmose, H. (2007), 'Violent breaking wave impacts. Part 1: Results from large-scale regular wave tests on vertical and sloping walls', *Coastal Engineering* **54**, 602–617.
URL: *http://dx.doi.org/10.1016/j.coastaleng.2006.12.002*

Gu, H., Qian, L., Causon, D., Mingham, C. & Lin, P. (2014), 'Numerical simulation of water impact of solid bodies with vertical and oblique entries', *Ocean Engineering* **75**, 128–137.
URL: *http://dx.doi.org/10.1016/j.oceaneng.2013.11.021*

Hou, G., Wang, J. & Layton, A. (2012), 'Numerical methods for fluid-structure interaction — a reviewjasa', *Communications in Computational Physics* **12**, 337–377.
URL: *http://dx.doi.org/10.4208/cicp.291210.290411s*

Jasak, H. (1996), Error analysis and estimation for the finite volume method with applications to fluid flows, PhD thesis, University of London.

Jasak, H. & Weller, H. G. (2000), 'Application of the finite volume method and unstructured meshes to linear elasticity', *International Journal for Numerical Methods in Engineering* **48**, 267–287.

Kissling, K., Springer, J., Jasak, J., Schutz, S., Urban, K. & Piesche, M. (2010), A coupled pressure based solution algorithm based on the volume-of-fluid approach for two or more immiscible fluids, *in* 'Proceedings of the V European Conference on Computational Fluid Dynamics, ECCOMAS CFD'.

Liao, K., Hu, C. & Duan, W. (2013), 'Two-dimensional numerical simulation of an elastic wedge water entry by a coupled FDM-FEM method', *Journal of Marine Science and Application* **12**, 163–169.
URL: *http://dx.doi.org/10.1007/s11804-013-1181-2*

Liao, K., Hu, C. & Sueyoshi, M. (2014), Numerical simulation of free surface flow impacting on an elastic plate, *in* '29th International Workshop on Water Waves and Floating Bodies'.

Liao, K., Hu, C. & Sueyoshi, M. (2015), 'Free surface flow impacting on an elastic structure: Experiment versus numerical simulation', *Applied Ocean Research* **50**, 192–208.
URL: *http://dx.doi.org/10.1016/j.apor.2015.02.002*

Lu, C., HE, Y. & WU, G. (2000), 'Coupled analysis of nonlinear interaction between fluid AND structure during impact', *Journal of Fluids and Structures* **14**, 127–146.
URL: *http://dx.doi.org/10.1006/jfls.1999.0257*

Lugni, C., Bardazzi, A., Faltinsen, O. M. & Graziani, G. (2014), 'Hydroelastic slamming response in the evolution of a flip-through event during shallow-liquid sloshing', *Physics of Fluids* **26**(3), 032108.
URL: *http://dx.doi.org/10.1063/1.4868878*

Lugni, C., Brocchini, M. & Faltinsen, O. M. (2010), 'Evolution of the air cavity during a depressurized wave impact. II. The dynamic field', *Phys. Fluids* **22**, 056102.
URL: *http://dx.doi.org/10.1063/1.3409491*

Ma, Z., Causon, D., Qian, L., Mingham, C. & Martínez Ferrer, P. (2016), 'Numerical investigation of air enclosed wave impacts in a depressurised tank', *Ocean Engineering* **123**, 15–27.
URL: *http://dx.doi.org/10.1016/j.oceaneng.2016.06.044*

Martínez Ferrer, P., Causon, D., Qian, L., Mingham, C. & Ma, Z. (2016*a*), 'A multi-region coupling scheme for compressible and incompressible flow solvers for two-phase flow in a numerical wave tank', *Computers & Fluids* **125**, 116–129.
URL: *http://www.sciencedirect.com/science/article/pii/S004579301500376X*

Martínez Ferrer, P. J., Causon, D. M., Qian, L., Mingham, C. G. & Ma, Z. H. (2016*b*), Numerical simulation of wave slamming on a flap type oscillating wave energy device, *in* 'Proceedings of the 26th International Ocean and Polar Engineering Conference', pp. 672–677.

Rusche, H. (2002), Computational fluid dynamics of dispersed two-phase flows at high phase fractions, PhD thesis, University of London.

Tukovic, Z., Ivankovic, A. & Karac, A. (2013), 'Finite-volume stress analysis in multi-material linear elastic body', *International Journal for Numerical Methods in Engineering* **93**, 400–419.
URL: *http://dx.doi.org/10.1002/nme.4390*

Tukovic, Z. & Jasak, H. (2007), 'Updated Lagrangian finite volume solver for large deformation dynamic response of elastic body', *Transactions of FAMENA* **31**, 55–70.

Weller, H. (2002), Derivation, modelling and solution of the conditionally averaged two-phase flow equations, Technical report, Nabla Ltd, No Technical Report TR/HGW/02.

Zhao, R. & Faltinsen, O. (1993), 'Water entry of two-dimensional bodies', *Journal of Fluid Mechanics* **246**, 593–612.
URL: *http://dx.doi.org/10.1017/S002211209300028X*